1778 *Biochemistry* **2011,** *50,* 1778–1787
DOI: 10.1021/bi1014562

BIOCHEMISTRY
including biophysical chemistry & molecular biology
Article

Identification of N-Terminal Regions of Wheat Leaf Ferredoxin NADP$^+$ Oxidoreductase Important for Interactions with Ferredoxin[†]

C. G. Bowsher,*[,‡] L. M. Eyres,[‡] J. O. Gummadova,[‡] P. Hothi,[§] K. J. McLean,[§] A. W. Munro,[§] N. S. Scrutton,[§] G. T. Hanke,[∥] Y. Sakakibara,[∥] and T. Hase[∥]

[‡]*Faculty of Life Sciences, The University of Manchester, Michael Smith Building, Manchester M13 9PT, U.K.,* [§]*Faculty of Life Sciences, Manchester Interdisciplinary Biocentre, The University of Manchester, Manchester M1 7DN, U.K., and* [∥]*Division of Protein Chemistry, Institute for Protein Research, 3-2 Yamadaoka, Suita, Osaka 565-0879, Japan*

Received September 9, 2010; Revised Manuscript Received January 25, 2011

ABSTRACT: Wheat leaves contain two isoproteins of the photosynthetic ferredoxin:NADP$^+$ reductase (*p*FNRI and *p*FNRII). Truncated forms of both enzymes have been detected *in vivo*, but only *p*FNRII displays N-terminal length-dependent changes in activity. To investigate the impact of N-terminal truncation on interaction with ferredoxin (Fd), recombinant *p*FNRII proteins, differing by deletions of up to 25 amino acids, were generated. During purification of the isoproteins found *in vivo*, the longer forms of *p*FNRII bound more strongly to a Fd affinity column than did the shorter forms, *p*FNRII$_{ISKK}$ and *p*FNRII[N−2]$_{KKQD}$. Further truncation of the N-termini resulted in a *p*FNRII protein which failed to bind to a Fd column. Similar k_{cat} values (104−140 s^{-1}) for cytochrome *c* reduction were measured for all but the most truncated *p*FNRII[N−5]$_{DEGV}$, which had a k_{cat} of 38 s^{-1}. Stopped-flow kinetic studies, examining the impact of truncation on electron flow between mutant *p*FNRII proteins and Fd, showed there was a variation in k_{obs} from 76 to 265 s^{-1} dependent on the *p*FNRII partner. To analyze the sites which contribute to Fd binding at the *p*FNRII N-terminal, three mutants were generated, in which a single or double lysine residue was changed to glutamine within the *in vivo* N-terminal truncation region. The mutations affected binding of *p*FNRII to the Fd column. Based on activity measurements, the double lysine residue change resulted in a *p*FNRII enzyme with decreased Fd affinity. The results highlight the importance of this flexible N-terminal region of the *p*FNRII protein in binding the Fd partner.

Ferredoxin NADP$^+$ oxidoreductase (FNR,[1] EC 1.18.1.2) catalyzes the reversible transfer of electrons between ferredoxin (Fd) and NADP$^+$. The biochemical properties of the FNR prosthetic group (flavin adenine dinucleotide, FAD) enable it to act as either a 2- or 1-electron donor/acceptor, taking or receiving 2 electrons from consecutive 1 electron carrier proteins, notably Fds, and passing these to NADP(H) (*1*). The variability of the redox potentials for the flavin prosthetic group between various FNRs means that they can participate in a range of different redox reactions and, as such, have been isolated from a variety of organisms exhibiting both phototrophic and heterotrophic metabolism and requiring the transfer of electrons in numerous biochemical processes (*2*).

In higher plant tissues, distinct photosynthetic (*p*FNR) and heterotrophic (*h*FNR) forms of FNR have been isolated and characterized. In photosynthetic tissue the last step of the photosynthetic electron transport chain involves the transfer of electrons to produce NADPH via the action of *p*FNR (*1*, *3*). The presence of multiple forms of *p*FNR may have an important role in regulating different metabolic requirements of the plant and may influence the efficient movement of electrons, not only for photosynthesis but also for other aspects of metabolism including nitrogen assimilation and the response of plants to oxidative damage and salt stress (*4*−*8*).

In previous work, we identified the presence of multiple forms of *p*FNR in wheat leaves, *p*FNRI$_{KKVS}$, *p*FNRI$_{SKKQ}$, *p*FNRII$_{ISKK}$, and *p*FNRII$_{KKQD}$. These multiple forms have varied expression and N-terminal processing (*9*). Kinetic analysis of recombinant wheat *p*FNR proteins with these variations in N-terminal truncation, using either photosynthetic ferredoxin (FdI) or heterotrophic ferredoxin (FdIII), showed that N-terminal truncation of *p*FNRI had little effect on the K_m and k_{cat} values with either Fd form. The N-terminal variants of wheat *p*FNRI have been shown to have different roles in the partitioning of photosynthetic reductant (*6*). This may, at least in part, be related to N-terminal processing of *p*FNRI, which has also been identified as potentially important in thylakoid targeting (*6*). In contrast, recombinant *p*FNRII proteins had a 2-fold higher activity than *p*FNRI isoforms but considerably lower affinity for Fds when measured using a cytochrome *c* reduction assay system in the presence of a constant 20 nM *p*FNR and a range of Fd concentrations (*9*). Furthermore, the alternative N-terminal cleavage sites identified for *p*FNRII had a significant impact on

[†]L.M.E. is grateful to the BBSRC for support from the Wain fellowship. J.O.G. was funded by grants from the Open Society Institute (New York, USA) and the Central European University (Budapest, Hungary). Financial support from the BBSRC Japanese Partnership Award is gratefully acknowledged.

*Address correspondence to this author. Tel: (+44) 0161 275 3898. Fax: (+44) 0161 275 5082. E-mail: caroline.bowsher@manchester.ac.uk.

[1] *A*, absorbance; *E*, observed reduction potential; $E_{ox/sq}$, $E_{sq/red}$, and $E_{ox/red}$, midpoint reduction potentials for oxidized/semiquinone, semiquinone/reduced, and oxidized/reduced couples of flavin cofactor; Fd, ferredoxin; FNR, ferredoxin NADP$^+$ oxidoreductase; *h*FNR, heterotrophic ferredoxin NADP$^+$ oxidoreductase; NHE, normal hydrogen electrode; ox, oxidized; *p*FNR, photosynthetic ferredoxin NADP$^+$ oxidoreductase; red, reduced.

 Published on Web 01/25/2011

its interaction with Fd. That is, the longer form of *p*FNRII$_{ISKK}$ was able to discriminate between the photosynthetic FdI and the heterotrophic FdIII, while a two amino acid N-terminal truncation to *p*FNRII$_{KKQD}$ eliminated this discrimination, making the K_m for FdI equivalent to that for FdIII (*9*). In previous work the highly homologous maize FdI and FdII were found to have critical amino acid substitutions leading to a difference in their ability to interact with *p*FNR (*10*). When these different maize Fd isoforms were overexpressed in *Plectonema boryanum*, the cyanobacterium showed significant differences in its electron partitioning ability between cyclic electron transport and nitrate assimilation (*11*). Recent analysis of mutant *Arabidopsis* plants grown under adverse conditions has suggested an important role for *p*FNRI in supplying electrons to different reducing pathways (*5*). Discrimination between Fd forms by truncation of wheat *p*FNRII could provide the leaf with the flexibility to respond to changes in reductant and, depending on the photosynthetic status of the cell, alter the balance between the cyclic and linear electron flow pathways.

A combination of biochemical and crystallographic studies has contributed to our understanding of the structure and enzyme mechanism of *p*FNR (*1*). Protein−protein interaction between Fd and *p*FNR is an important determinant of electron transfer between the redox centers of these proteins. Many of the residues responsible for orientating the proteins and stabilizing the complex were initially identified in extensive site-directed mutagenesis studies (*12*−*14*). These findings were subsequently confirmed by the solution of crystal structures of complexes between Fd and FNR from both *Anabaena* (*15*) and maize (*16*). There is considerable variation between the orientation of Fd in the FNR active site in these two structures, but the basic principle remains the same. Hydrophobic patches surrounding the redox centers of each protein form a contact site from which water is excluded, while the orientation of the complex is stabilized by a series of ionic interactions between charged side chains that surround this area. In the maize *p*FNR:Fd complex, an intramolecular salt bridge in Fd is broken in favor of an intermolecular salt bridge (*16*), probably resulting in a negative shift of the redox potential (*17*, *18*). The maize complex structure clearly identified interacting residues around the rigid core of the protein, but the N-terminus had a lower resolution and was not clearly visible (*16*). The N-terminus of the *p*FNR has been identified as a long, highly flexible, disordered tail (*19*). Chemical modification studies identified residues in the N-terminal region of *p*FNR that were potentially important in its interaction with Fd (*20*, *22*). Furthermore, NMR analysis, together with the use of N-terminal truncated mutants of maize leaf *p*FNR overexpressed in *Escherichia coli*, has confirmed the importance of this flexible N-terminal region for binding Fd (*19*). More specifically, the motifs EAxxPA and KxSKK in the N-terminal region of *p*FNR have been identified as being important for Fd binding (*19*).

This paper further investigates the impact of truncating the N-terminal region of *p*FNRII. In particular, we have examined the ability of *p*FNRII with different N-terminal region lengths to bind FdI and to support electron flow. Such information provides an insight into the importance of this flexible N-terminal region of the *p*FNR protein in regulating metabolism.

EXPERIMENTAL PROCEDURES

Preparation of Overexpressed pFNRII. The wheat *p*FNRII cDNA clones (*9*) were used as templates to generate PCR products with alternative lengths of the corresponding *p*FNR gene. The sense PCR primers were designed to be complementary to the 5′ end of the truncation site and to incorporate an *Nco*I or *Bsp*HI restriction enzyme site (underlined). The sense primers were as follows: *p*FNRII[N+22]$_{AQVS}$, 5′GGCGCCATGGCTCAAGTATCAACTACC GAGCCGACCGCGGA3′; *p*FNRII[N+8]$_{AAPA}$, 5′GCGCCATGGCAGCACCAGCAAAACCGGTG AAGATCTCCAAG3′; *p*FNRII[N+2]$_{VKIS}$, 5′GGCGCCATGGTTAAAATATCTAAAAAAC AGGACGGGGGTGGTG3′; *p*FNRII$_{ISKK}$, 5′GGCGTCATGAATTTCTAAGAAACAAGATGAAGGT GTGGTGACCAACAAG3′; *p*FNRII[N−2]$_{KKQD}$, 5′GGCGCCATGGGTTAAAAAACAAGATGAA GGGGTGGTGACCAACAAG3′; *p*FNRII[N−5]$_{DEGV}$, 5′GGCGCCATGGATGAAGGTGTAACTAAC AAGTACCGCCCCAAG3′.

In all cases the same antisense primer was used which was complementary to the 3′ end of the *p*FNR gene and incorporated the *Bam*HI restriction enzyme site (underlined) which is downstream of the stop codon for the *p*FNRII gene: 5′TAAGGATCCGATGATGATAATCAGTAGACTTCG3′.

The PCR reaction was hot started at 94 °C for 30 s and carried out for 25 cycles at 94 °C for 30 s, 62 °C for 30 s, and 72 °C for 90 s. This was followed by a final incubation at 72 °C for 7 min, prior to storage at 4 °C. The resulting PCR products were cloned into the pQE60 vector and overexpressed with either the TG1 or JM109 *E. coli* strains, as described previously (*23*).

Site-Directed Mutagenesis. For the preparation of *p*FNRII forms with altered lysine residues, a site-directed mutagenesis approach was undertaken. In all cases the longest *p*FNRII plasmid (*p*FNRII[N+22] $_{AQVS}$) was used as the template to generate the PCR products corresponding to the mutagenized *p*FNRII gene, where specific lysine residues were changed to glutamine residues (bold). The forward and reverse primers to generate *p*FNRII[N+22]$_{AQVS}$ $K^{+1}Q$ were 5′GCTAAACCTGTG**CAG**ATCTCCAAGAAG3′ and 5′CTTCTTGGAGAT**CT**GCACAGGTTTAGC3′, respectively; to generate *p*FNRII[N+22]$_{AQVS}$ $K^{-2}Q$ these were 5′GTGAAGATCTCC**CAG**AAGCAGGACGAGGGG3′ and 5′CCCCTCGTCCTGCTT**CT**GGGAGATCTTCAC3′, respectively; and to generate *p*FNRII[N+22]$_{AQVS}$ $K^{-2-3}QQ$ these were 5′GTGAAGATCTCC**CAGCAG**CAGGACGAGGGG3′ and 5′CCCCTCGTCCTG**CTGCTG**GGAGATCTTCAC3′, respectively. The PCR reactions were hot started at 95 °C for 60 s and carried out for 18 cycles at 95 °C for 50 s, 60 °C for 50 s, and 68 °C for 3 min, followed by 1 cycle at 68 °C for 7 min, prior to storage at 4 °C.

Purification of Overexpressed pFNRII Forms Using a Ferredoxin Affinity Column. All recombinant forms of *p*FNRII proteins were purified as described by Gummadova et al. (*9*). A maize FdI-affinity column was used for the final step of the purification (*23*), and elution of *p*FNRII proteins was monitored by absorbance at 280 nm using an AKTA Prime system (Pharmacia Biotech).

Enzyme Assays. Catalytic activities of the alternative forms of *p*FNRII were determined using a cytochrome *c* reduction assay, as described previously (*9*, *23*). When determining the NADPH-dependent cytochrome *c* reductase activity of *p*FNR, the cytochrome *c* (200 μM) and enzyme (20 nM) concentrations remained constant, while a range of FdI concentrations were used in the presence of 50 mM Tris-HCl, pH 7.5. The data were fitted using the Michaelis−Menten equation. The kinetic constants K_m and k_{cat} were calculated by plotting the rate data versus the relevant FdI concentration and fitting using a hyperbolic

function and nonlinear regression analysis with Origin software (OriginLab, Northampton, MA).

Sample Preparation for Stopped-Flow Kinetic Studies. Anaerobic procedures were performed in an anaerobic glovebox (Belle Technology, Portesham, England) with < 5 ppm oxygen. The buffer was made anaerobic by bubbling with argon for 2 h and then allowed to equilibrate overnight in the glovebox. Anaerobic solutions of sodium dithionite were prepared by dissolving preweighed solid in anaerobic buffer. Enzymes were exchanged into anaerobic 50 mM Tris buffer, pH 8.0, by gel exclusion chromatography. Absorbance changes during redox titrations were followed spectroscopically using a Jasco V-550 UV/vis spectrophotometer housed in the glovebox.

Stopped-Flow Kinetic Studies. Rapid kinetic experiments were performed using an Applied Photophysics SX 18MV stopped-flow spectrophotometer housed in a glovebox. Studies of electron transfer from FdI to *p*FNR were performed by rapid mixing of oxidized *p*FNRII ($pFNRII_{ox}$, 2.5 μM reaction cell concentration) with various concentrations of reduced FdI (Fd_{red}, see Results) in 50 mM Tris buffer, pH 8.0, at 4 °C. The pH was established as near optimal for the enzyme activity. FdI was stoichiometrically reduced (in the presence of 0.3 μM methyl viologen) with sodium dithionite. To prevent the accumulation of excess dithionite, the concentration of dithionite was determined by titration with a FAD stock of known concentration. The increase in absorbance, representing oxidation of Fd_{red}, was followed at 522 nm. This wavelength was chosen as there is a large absorbance change between oxidized and reduced forms of the Fd and a relatively small absorbance change between the FAD cofactor in its hydroquinone and semiquinone forms. In the single turnover reaction we thus examined the single electron transfer from *p*FNR protein to the Fd, with the overall absorption change indicating the concomitant oxidation and reduction of the proteins. Data were analyzed by nonlinear least-squares regression analysis on an Acorn RISC PC using Spectrakinetics software (Applied Photophysics). For each reaction, at least three replicate measurements were collected and averaged, each containing 1000 data points. The observed absorbance change was best fitted to a triphasic exponential expression. For studies of electron transfer from $pFNRII_{red}$ enzymes to Fd, *p*FNRII proteins (2.5 μM reaction cell concentration) were stoichiometrically reduced with sodium dithionite, in the presence of 0.3 μM methyl viologen, and rapidly mixed with various concentrations of Fd_{ox} at 4 °C. Methyl viologen was present in catalytic amounts as a mediator of electron transfer from dithionite to the protein. In control experiments we established that methyl viologen did not contribute significantly to any absorbance changes associated with Fd/FNR electron transfer reactions. The decrease in absorbance was followed at 522 nm, representing reduction of Fd_{ox}. Absorbance changes were monophasic, and observed rates were obtained by fitting to a standard single exponential expression. No changes were observed between reaction transients collected in the presence or absence of glucose oxidase.

Redox Titrations of pFNRII Proteins. Redox titrations to determine potentials for the FAD cofactor in the *p*FNRII proteins were carried out in an anaerobic glovebox (Belle Technology) under a nitrogen atmosphere, with oxygen levels maintained at < 5 ppm. Redox titrations were carried out for each of the *p*FNRII proteins (typically 25−50 μM protein) and for the Fd (65 μM) at 25 ± 2 °C using the method of Dutton and essentially as described previously (*24*−*26*). Redox titration buffer (100 mM potassium phosphate, pH 7.0, to obtain potential values under standard conditions) was deoxygenated by bubbling extensively with O_2-free argon and degassed prior to transfer to the glovebox. Oxygen was removed from protein samples by passing concentrated stock solutions through a Bio-Rad Econo-pac 10DG gel filtration column in the glovebox, which had been preequilibrated with redox titration buffer containing 5% (v/v) glycerol. Enzymes were titrated with sodium dithionite as a reductant and potassium ferricyanide as an oxidant. Dithionite and ferricyanide were delivered in approximately 1−2 μL aliquots from concentrated stock solutions (typically 10−50 mM). Titrations were performed in both reductive and oxidative directions to ensure lack of hysteresis. Absorption changes during the titrations were monitored via a fiber optic absorption probe (Varian) immersed in the protein solution in the anaerobic environment and connected to a Cary UV-50 Bio UV−visible spectrophotometer (Varian) outside the glovebox. Potentials were measured using a Hanna pH 211 m coupled to a Pt/calomel electrode (ThermoRussell Ltd.) at 25 ± 2 °C. The electrode was calibrated using the Fe^{3+}/Fe^{2+} EDTA couple as a standard (+108 mV). A factor of +244 mV was used to correct relative to the standard hydrogen electrode. Mediators were added to facilitate electrical communication between enzyme and electrode, prior to titration. Two micromolar phenazine methosulfate, 5 μM 2-hydroxy-1,4-naphthoquinone, 0.5 μM methyl viologen, and 1 μM benzyl viologen were included to mediate in the range between +100 and 480 mV, as described previously (*25*, *26*). The electrode was allowed to stabilize between each addition of reductant/oxidant prior to spectral acquisition and recording of the potential.

Data were analyzed by plotting absorbance at an appropriate wavelength, corresponding to a maximal absorbance change between oxidized and reduced forms of the proteins, against the applied potential. A 2-electron Nernst function (eq 1) was then used to fit the data, to describe the transitions between quinone, semiquinone, and hydroquinone forms of the *p*FNRII FAD cofactors, and to calculate the midpoint potentials for the cofactors from these data fits. Equation 1 represents a 2-electron redox process derived by extension to the Nernst equation and the Beer−Lambert law, as described previously (*24*−*27*).

$$A = \frac{a10^{(E - E_{ox/sq})/59} + b + c10^{(E_{sq/red} - E)/59}}{1 + 10^{(E - E_{ox/sq})/59} + 10^{(E_{sq/red} - E)/59}} \quad (1)$$

In eq 1, A is the total absorbance of the *p*FNRII FAD; a, b, and c are component absorbance values contributed by the FAD in the oxidized, semiquinone, and reduced states; E is the observed potential; $E_{ox/sq}$ and $E_{sq/red}$ are the midpoint potentials for oxidized/semiquinone and semiquinone/reduced couples of the flavin, respectively.

The midpoint reduction potential for the iron sulfur cluster in the Fd was also determined using a single electron Nernst function (eq 2), as described previously (*28*).

$$A = \frac{a + b \times 10^{(E_{ox/red} - E)/59}}{1 + 10^{(E_{ox/red} - E)/59}} \quad (2)$$

In eq 2, A is the total absorption change, a and b are component absorbance values contributed by the Fd in the oxidized and reduced states; E is the observed potential and $E_{ox/red}$ is the midpoint potential for the reductive transition.

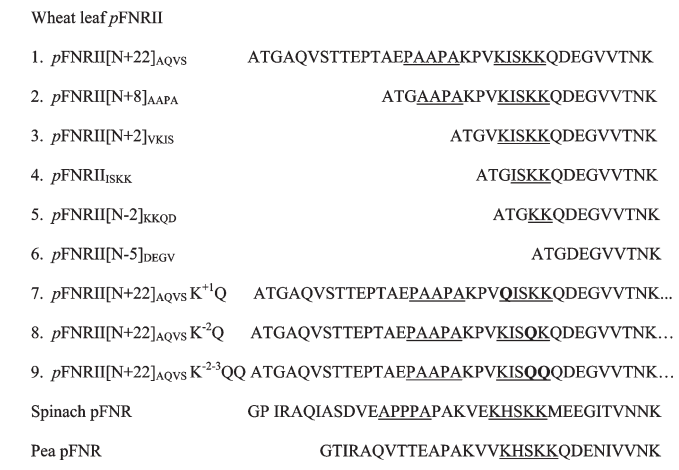

FIGURE 1: N-Terminal forms of *p*FNRII. Sequence alignment of the N-terminal regions of *p*FNRII. The underlined regions highlight the EAxxPA and KxSKK motifs. The deduced amino acid sequences for wheat (*9*), spinach (*40*), and pea (*41*) are shown.

RESULTS

Figure 1 shows the N-terminal sequences of the overexpressed forms of *p*FNRII used in this study. Based on alignment studies, the transit peptide of *p*FNRII is predicted to end with a conserved R/KxT/AxA/Q motif. In wheat, the mature N-terminal starts at 19−23 positions after the end of the transit peptide (*6*). The *p*FNRII[N+22]$_{AQVS}$ starts at the predicted end of the transit peptide. Based on the previous identification by Maeda et al. (*19*) of a potentially important EAxxPA motif in maize, *p*FNRII-[N+8]$_{AAPA}$, with an extended N-terminal region to include this motif, was generated. A KxSKK motif in the N-terminal region of maize *p*FNR has previously been identified as being important for Fd binding (*19*). From our own studies this has been further supported since N-terminal truncation within this motif generates the two *in vivo* forms of *p*FNRII: *p*FNRII$_{ISKK}$ and *p*FNRII$_{KKQD}$ (*9*). To investigate the importance of this region, an additional two amino acids were added to generate an N-terminal region with the full wheat KISKK domain, *p*FNRII-[N+2]$_{VKIS}$. In addition, a truncated N-terminal domain beginning after the KISKK domain, *p*FNRII[N−5]$_{DEGV}$, was also generated.

The same purification procedure was used for isolating the different overexpressed *p*FNRII forms, including Resource Q and phenyl-Sepharose chromatography prior to a final step employing a Fd affinity column. The salt concentration necessary for the elution of the different overexpressed *p*FNR forms from the Fd affinity column varied depending on the nature of the N-terminal region. *p*FNRII[N+22]$_{AQVS}$, *p*FNRII[N+8]$_{AAPA}$, and *p*FNRII[N+2]$_{VKIS}$ bound strongly to the Fd affinity column, being eluted between 270 and 370 mM NaCl. The overexpressed forms representing the known N-terminal cleavage sites for wheat (*p*FNRII$_{ISKK}$, *p*FNRII[N−2]$_{KKQD}$) bound less strongly and were eluted between 140 and 150 mM NaCl. Removal of additional amino acids led to a truncated form of *p*FNRII[N−5]$_{DEGV}$, that failed to bind to the Fd affinity column (data not shown). In the case of *p*FNRII[N−5]$_{DEGV}$, purification to homogeneity was achieved by replacing the Fd affinity column chromatography step with a Superdex 200 chromatography column step. The SDS−PAGE patterns of the alternative *p*FNRII forms overexpressed in *E. coli* show slightly different electrophoretic mobilities which reflect the truncations in the N-terminal regions (Supporting Information Figure S1A). Separation by native PAGE, followed by staining either with Coomassie Blue for total protein (data not shown) or with an FNR/diaphorase enzyme activity stain (Supporting Information Figure S1B), identified single bands with different mobilities for each alternative *p*FNRII form.

Table 1: Summary of the Effect of N-Terminal Truncation on the Catalytic Efficiency of *p*FNRII in an NADPH-Dependent Cytochrome *c* Reduction Assay[a]

*p*FNRII enzyme	k_{cat} (s^{-1})	K_m (μM)	k_{cat}/K_m (s^{-1} μM^{-1})
*p*FNRII[N+22]$_{AQVS}$	104.0 ± 4.1	3.12 ± 0.45	33.33
*p*FNRII[N+8]$_{AAPA}$	139.4 ± 8.8	11.03 ± 1.40	12.64
*p*FNRII[N+2]$_{VKIS}$	128.2 ± 5.3	9.99 ± 0.86	12.83
*p*FNRII[N−5]$_{DEGV}$	38.1 ± 2.3	10.30 ± 1.48	3.70

[a] *p*FNRII proteins with alternative N-terminal cleavage points were overexpressed in *E. coli*, purified, and assayed as described in Experimental Procedures. The data represent the mean of at least three independent experiments in each case. The *in vivo* N-terminal truncated forms *p*FNRII$_{ISKK}$ and *p*FNRII[N−2]$_{KKQD}$ have K_m values of 28.6 and 8.35 μM and a catalytic efficiency of 4.24 and 13.24 s^{-1} μM^{-1}, respectively, as previously reported (*9*).

A cytochrome *c* reduction assay was used to measure electron transfer from NADPH to Fd by the alternative forms of *p*FNRII, since reduction of the cytochrome is easily measured, and electron transfer from Fd_{red} to cytochrome *c* is rapid. Catalytic efficiency was determined in an assay, where the amounts of variably truncated *p*FNRII enzymes (20 nM) and cytochrome *c* (200 μM) were constant and the concentration of FdI was varied (0−40 μM). Results are summarized in Table 1. The lowest k_{cat} of 38.1 ± 2.3 s^{-1} was seen for the most truncated N-terminal form (*p*FNRII[N−5]$_{DEGV}$) and was markedly different from that determined for all of the longer forms of *p*FNRII, which ranged from 104.0 ± 4.2 s^{-1} with *p*FNRII[N+22]$_{AQVS}$ to 139.4 ± 8.8 s^{-1} for *p*FNRII[N+8]$_{AAPA}$ (Table 1). The longer form of *p*FNRII-[N+22]$_{AQVS}$ had the highest affinity with a K_m value of 3.12 ± 0.45 μM and the highest catalytic efficiency. Further N-terminal truncations resulted in *p*FNRII forms exhibiting similar K_m values of 9.99 ± 0.86 μM for *p*FNRII[N+2]$_{VKIS}$ to 11.03 ± 1.40 μM for *p*FNRII[N+8]$_{AAPA}$.

To investigate further the origins of the impact of *p*FNRII N-terminal truncations on k_{cat} and apparent affinity for FdI, stopped-flow kinetic studies were undertaken. Initially, data were collated from the spectral properties generated in titrations of oxidized *p*FNRII enzymes (see data for pFNRII[N−5]$_{DEGV}$ in Figure 2A) or for FdI (Figure 2B) with dithionite. This allowed selection of a suitable wavelength range of 520−530 nm to follow spectral changes reporting interprotein electron transfer during stopped-flow reactions (Figures 3 and 4). The observed rate constants determined from stopped-flow reactions with *p*FNRII forms and FdI ranged from 75.7 ± 0.9 s^{-1} with *p*FNRII-[N−5]$_{DEGV}$ to 259.2 ± 2.3 s^{-1} for *p*FNRII$_{ISKK}$ (Table 2). In these experiments, there was no significant variation in the k_{obs} determined across the Fd concentration range between 25 and 200 μM. This demonstrates that affinity of binding of Fd is retained in all cases, such that the limiting electron transfer rate is achieved by 25 μM Fd but that the electron transfer rate is affected considerably, possibly through nonoptimal orientation of Fd within the FNR binding site of the truncated *p*FNRII proteins and/or perturbations to the FAD potentials in these proteins.

For each of the *p*FNRII proteins, redox titrations demonstrated the conversion of the oxidized flavoprotein toward the

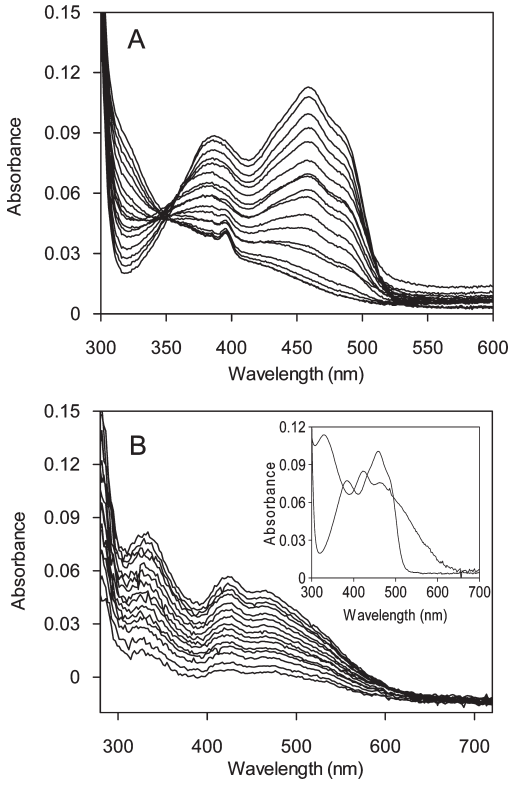

FIGURE 2: Spectral properties of *p*FNRs and ferredoxin. (A) Spectral changes accompanying the titration of oxidized *p*FNRII[N−5]$_{DEGV}$ protein with sodium dithionite. *p*FNRII[N−5]$_{DEGV}$ (~8 μM), contained in 50 mM Tris buffer (pH 8.0), was stoichiometrically reduced by the addition of sodium dithionite under strict anaerobic conditions at 25 °C. Absorbance decrease across the spectrum accompanies FAD cofactor reduction. (B) As for panel A but for the reduction of oxidized ferredoxin (~4 μM). Again, spectrum-wide absorbance decrease occurs as the iron−sulfur cluster is reduced. Inset: superimposed spectra of *p*FNRII[N−5]$_{DEGVox}$ and ferredoxin$_{ox}$, identifying suitable wavelengths (i.e., 520−530 nm) to follow redox-dependent absorbance changes during stopped-flow reactions.

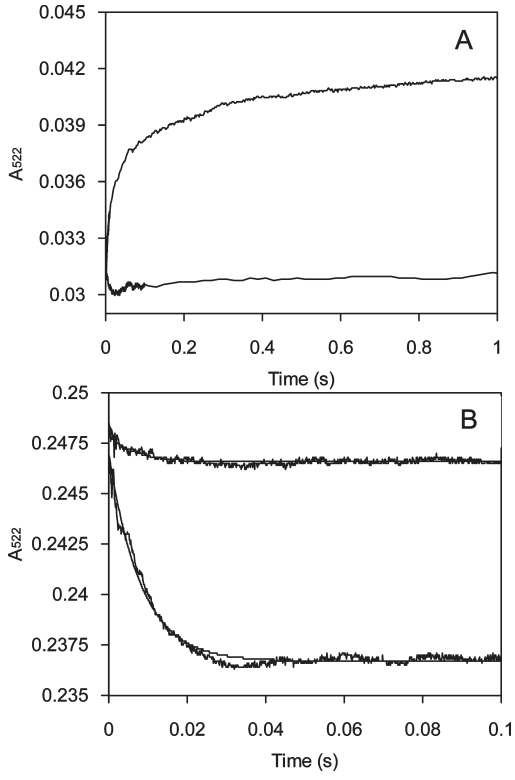

FIGURE 3: Stopped-flow kinetic transients for the reactions of pFNRII$_{ISKK}$ and ferredoxin. (A) An example of the triphasic absorbance change observed during reactions of ferredoxin$_{red}$ (25 μM reaction cell concentration) versus oxidized *p*FNRII$_{ISKK}$ (2.5 μM). The increase in absorbance corresponds to oxidation of reduced ferredoxin. The control (25 μM ferredoxin$_{red}$ versus 50 mM Tris buffer, pH 8.0, in the absence of *p*FNRII$_{ISKK}$) demonstrates the significant amplitude change observed on mixing of ferredoxin$_{red}$ with *p*FNRII$_{ox}$. The observed rate constant for the third phase (k_3 ~ 1 s^{-1}) is similar to the rate of ferredoxin reoxidation and thus represents a background reaction. The rate of the third phase is significantly lower than that for k_1 (~200 s^{-1}; Figure 4A and Table 2) and k_2 (~25 s^{-1}) and can thus be ignored. (B) An example of the monophasic absorbance change observed during reactions of reduced *p*FNRII$_{ISKK}$ (2.5 μM reaction cell concentration) with ferredoxin$_{ox}$ (50 μM). The decrease in absorbance corresponds to reduction of oxidized ferredoxin. The control (2.5 μM reduced *p*FNRII$_{ISKK}$ versus 50 mM Tris buffer, pH 8.0, in the absence of ferredoxin) demonstrates the significant amplitude change on mixing of the two proteins. The observed rate constants (Figure 4B) are comparable to those of k_1 for reactions of ferredoxin$_{red}$ with *p*FNRII$_{ox}$.

reduced (hydroquinone) form with intermediate formation of the 1 electron reduced semiquinone species. In all cases there was development, and then decay, of a species with a broad absorption band between ~500 and 700 nm during the reductive phase of the titration. This absorption band is diagnostic for a neutral (protonated) blue semiquinone form. The redox titrations incorporate mediators to expedite electrical communication between enzyme and electrode, and the formation of semiquinone in these experiments indicates that the presence of mediators relieves a kinetic block to semiquinone formation in titrations of the *p*FNR proteins with dithionite. The absence of any notable absorption increase at ~400 nm indicated that there was negligible formation of any of the anionic semiquinone form in any of these enzymes during redox titration. A clear isosbestic point is seen in each titration at approximately 507 nm during the first phase of the redox titration associated with the oxidized/blue semiquinone redox transition. Spectra deviate from this isosbestic point during the semiquinone/hydroquinone transition, and decreasing absorption at approximately 600 nm demonstrates the reduction of the semiquinone to the hydroquinone in this final phase of the redox titrations. In all cases, the potentiometric titrations were essentially completed within the accessible potential range for dithionite (E_m ~ −420 mV), and data were fitted well using eq 1 and using the absorption change at the maximum for the oxidized enzyme. All data are presented in Table 3, with the midpoint potential for the 2-electron reduction in the range from −221 to −261 mV versus the normal hydrogen electrode (NHE) in all cases. Exemplary data for spectral changes observed are shown in Figure 5 for the spectral changes and for the associated data fits in the case of *p*FNRII[N+22]$_{AQVS}$ and *p*FNRII[N−2]$_{KKQD}$ enzymes. For the Fd, the redox potential (−440 ± 8 mV) is considerably more negative than for any of the *p*FNRII proteins, indicating that electron transfer in the direction of FAD reduction in the *p*FNRII proteins is thermodynamically favored.

The truncations result in some perturbations to the thermodynamic properties of the FNR FAD cofactors, presumably due to distortion of the protein environment around the FAD moiety (Table 3). Moreover, the stabilization of *p*FNRII blue semiquinones during the redox titration (for each *p*FNRII isoform) is clearly distinct from the anaerobic titration data with dithionite shown for the *p*FNRII[N−5]$_{DEGV}$ enzyme in the absence of

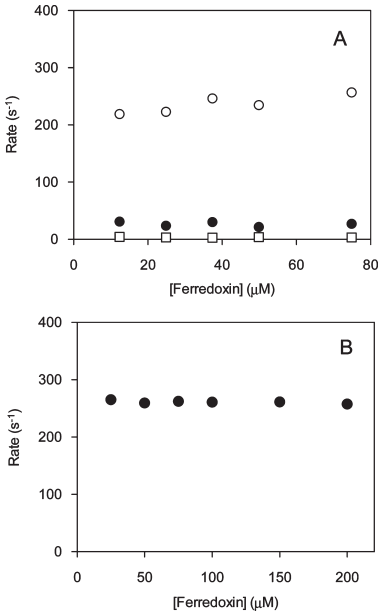

FIGURE 4: Stopped-flow kinetic data for the reaction of pFNRII$_{ISKK}$ and ferredoxin. (A) Observed rate constants from reactions of oxidized pFNRII$_{ISKK}$ (2.5 μM reaction cell concentration) with various concentrations of ferredoxin$_{red}$ (as described in Experimental Procedures). Key: open circles, k_1; closed circles, k_2; open squares, k_3. Observed rates were obtained by fitting to a triphasic exponential expression (Figure 3A). (B) Observed rate constants from reactions of reduced pFNRII$_{ISKK}$ (2.5 μM reaction cell concentration) with various concentrations of ferredoxin$_{ox}$ (as described in Experimental Procedures). Key: open circles, k_1; closed circles, k_2; open squares, k_3. Observed rates were obtained by fitting to a standard single exponential expression (Figure 3B). Ferredoxin$_{red}$ = reduced Fd.

Table 2: Observed Rate Constants (k_{obs}) Determined from Stopped-Flow Reactions of Reduced pFNR and Oxidized Ferredoxin at 4 °C[a]

pFNRII enzyme	k_{obs} (s^{-1})
pFNRII[N+22]$_{AQVS}$	143.6 ± 1.1
pFNRII[N+8]$_{AAPA}$	111 ± 1.2
pFNRII[N+2]$_{VKIS}$	200.4 ± 1.3
pFNRII$_{ISKK}$	259.2 ± 2.3
pFNRII[N−2]$_{KKQD}$	264.6 ± 3.4
pFNRII[N−5]$_{DEGV}$	75.7 ± 0.9

[a]In all cases, there was no apparent dependence of k_{obs} for ferredoxin reduction on varying the concentration of the ferredoxin protein under pseudo-first-order conditions. All reaction transients fitted well to a monoexponential function. An example of these kinetic data is shown in Figure 3B for the pFNRII$_{ISKK}$ enzyme.

mediators (Figure 2A), where there appears to be little blue semiquinone observed. This likely reflects a kinetic block to semiquinone formation on reduction with dithionite that is relieved with addition of the mediators. The 2-electron midpoint potential is more positive than that for the *E. coli* NADPH-dependent flavodoxin/ferredoxin reductase (FLDR, −288 ± 4 mV) (*29*). In this related *E. coli* flavoprotein, negligible amounts of blue semiquinone were formed in equilibrium redox titration as a consequence of the close proximity of the ox/sq and sq/hq couples. For the wheat pFNRII proteins, these couples were well separated, and substantial amounts of semiquinone were formed in all cases.

In previous studies, a number of lysine residues have been identified as being critical to the functioning of pFNR enzymes (*20*, *22*, *30*, *31*). Clearly, the region of the KISKK motif

Table 3: Redox Potentials for pFNRII Proteins[a]

	redox potential (mV versus NHE)		
pFNRII enzyme	$E_{ox/sq}$ (ox/sq)	$E_{sq/red}$ (sq/hq)	$E_{ox/red}$ (ox/hq)
pFNRII[N+22]$_{AQVS}$	−119 ± 5	−322 ± 4	−221 ± 5
pFNRII[N+8]$_{AAPA}$	−174 ± 13	−335 ± 7	−255 ± 10
pFNRII[N+2]$_{VKIS}$	−150 ± 6	−321 ± 4	−236 ± 5
pFNRII$_{ISKK}$	−186 ± 10	−335 ± 5	−261 ± 8
pFNRII[N−2]$_{KKQD}$	−132 ± 5	−329 ± 4	−230 ± 5
pFNRII[N−5]$_{DEGV}$	−128 ± 6	−325 ± 4	−227 ± 5

[a]Midpoint (2 electron, ox/hq, $E_{ox/red}$) reduction potentials and single electron (ox/sq, $E_{ox/sq}$, and sq/hq, $E_{sq/red}$) potentials were determined as described in the Experimental Procedures section. Values cited are relative to the normal hydrogen electrode (NHE).

in wheat pFNRII, which is critical to the K_m for Fd, also has several lysines. To investigate the importance of these residues and to further analyze the impact of N-terminal truncation upon binding of Fd, a site-directed mutagenesis approach was used. Targeting the wheat KISKK domain, which is the motif covering the region of the alternative mature N-terminal pFNRII start positions, we prepared three forms of pFNRII[N+22]$_{AQVS}$ where single lysine residues were changed to glutamine (Figure 1). The mutations had little effect on the mass of the proteins or their electrophoretic mobility based on SDS−PAGE (lanes 7−9, Supporting Information Figure S1A) or native PAGE (lanes 7−9, Supporting Information Figure S1B). However, binding of the different forms of pFNRII to the Fd-immobilized columns was influenced, with pFNRII[N+22]$_{AQVS}$ K^{-2-3}QQ, pFNRII-[N+22]$_{AQVS}$ K^{+1}Q, and pFNRII[N+22]$_{AQVS}$ K^{-2}Q being eluted at 120, 175, and 210 mM NaCl, respectively, in comparison to the wild-type form pFNRII[N+22]$_{AQVS}$, which was eluted at 250 mM NaCl (data not shown). Interestingly, although spectra of all the different forms of pFNRII (whether lengthened, truncated or mutated) were generally very similar, pFNRII-[N+22]$_{AQVS}$ K^{-2-3}QQ exhibited a shift of the longer wavelength flavin peak from 458 to 444 nm (data not shown), likely indicating a considerable change in the local environment of the isoalloxazine ring portion of the FAD cofactor. When the maximal catalytic rates (k_{cat} values) for cytochrome c reduction were compared with that for the wild-type form, pFNRII-[N+22]$_{AQVS}$, these were seen to decrease from 104.0 s^{-1} to 65.0 s^{-1} (pFNRII[N+22]$_{AQVS}$ K^{+1}Q), 66.3 s^{-1} (pFNRII[N+22]$_{AQVS}$ K^{-2}Q), and 45.4 s^{-1} (pFNRII[N+22]$_{AQVS}$ K^{-2-3}QQ; Table 4). The apparent K_m for FdI was largely unaffected by the single lysine changes, but the double lysine-to-glutamine mutation resulted in an increase in the FdI K_m from 3.1 μM (wild-type pFNRII) to 10.0 μM (pFNRII[N+22]$_{AQVS}$ K^{-2-3}QQ). The catalytic efficiency for the wild-type form, pFNRII[N+22]$_{AQVS}$, was similar to that for pFNRII[N+22]$_{AQVS}$ K^{+1}Q but reduced for pFNRII[N+22]$_{AQVS}$K^{-2}Q. The double lysine-to-glutamine mutant pFNRII[N+22]$_{AQVS}$ K^{-2-3}QQ had a catalytic efficiency similar to that of pFNRII[N−5]$_{DEGV}$ (Tables 1 and 4).

DISCUSSION

In higher plants pFNR has been characterized in detail at the primary and secondary structure level using sequence information gained, in part, from identifying and isolating various cDNA clones. Furthermore, a range of techniques including partial proteolysis (*21*, *22*, *32*), chemical modification (*22*, *30*, *31*, *33*, *34*), site-directed mutagenesis (*20*, *35*), and crystallography (*15*, *16*)

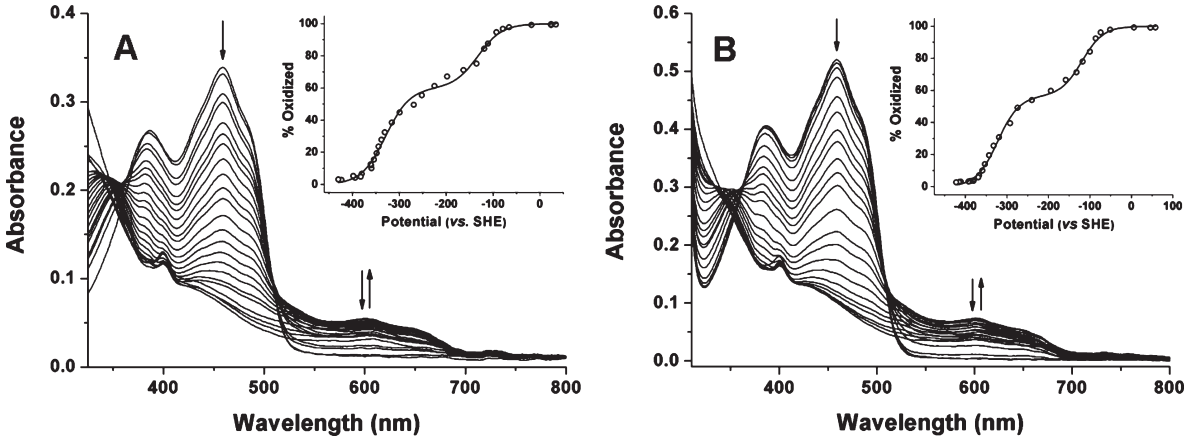

FIGURE 5: Spectral features and potentiometric data fits for wheat *p*FNRII proteins. (A) Spectral data accumulated during a redox titration of the *p*FNRII[N−2]$_{KKQD}$ flavoprotein (37 μM). (B) The parallel data set for the *p*FNRII[N+22]$_{AQVS}$ flavoprotein (56 μM). Arrows show directions of absorption change during the reductive phase of the redox titration, with clear accumulation of a blue neutral semiquinone species with absorption maximum at ~600 nm. The insets in each panel are the data fits using eq 1, giving midpoint redox potential values (vs NHE) of $E_{ox/sq} = -119 \pm 5$ mV, $E_{sq/red} = -322 \pm 4$ mV, and $E_{ox/red} = -221 \pm 5$ mV for *p*FNRII[N+22]$_{AQVS}$ and $E_{ox/sq} = -132 \pm 5$ mV, $E_{sq/red} = -329 \pm 4$ mV, and $E_{ox/red} = -230 \pm 5$ mV for *p*FNRII[N−2]$_{KKQD}$.

Table 4: Summary of Effect of Site-Directed Mutagenesis on Catalytic Efficiency of *p*FNRII [N+22]$_{AQVS}$ in a NADPH-Dependent Cytochrome *c* Reduction Assay[a]

*p*FNRII enzyme	k_{cat} (s^{-1})	K_m (μM)	k_{cat}/K_m ($s^{-1}\,\mu M^{-1}$)
*p*FNRII[N+22]$_{AQVS}$ $K^{+1}Q$	65.0 ± 1.5	2.05 ± 0.21	31.71
*p*FNRII[N+22]$_{AQVS}$ $K^{-2}Q$	66.3 ± 2.9	3.50 ± 0.57	18.94
*p*FNRII[N+22]$_{AQVS}$ $K^{-2-3}QQ$	45.4 ± 5.3	10.04 ± 3.16	4.52

[a] *p*FNRII proteins with alternative N-terminal cleavage points were overexpressed in *E. coli*, purified, and assayed as described in Experimental Procedures. The data represent the mean of at least three independent experiments in each case.

have all contributed to a clearer understanding of the roles of specific protein regions and amino acids in maintaining the structural integrity, substrate/cofactor docking and binding, and involvement in the transfer of electrons between Fd redox partners and NADP(H). In particular, recent NMR studies have allowed a more comprehensive appreciation of the contribution to cofactor and coenzyme binding at the distinct FAD binding domain of the N-terminus and at the NADP(H) binding domain of the C-terminus (*19*).

Fd binds within a large shallow cleft between the two domains of *p*FNR proteins (*17*, *36*). From a combination of biochemical approaches it has been possible to identify amino acid residues/regions that are involved in binding Fd to a variety of *p*FNR forms. In previous work using chemical modification studies (*33*, *34*), chemical cross-linking of Fd to *p*FNR, limited proteolysis of *p*FNR (*21*), and site-directed mutagenesis (*13*, *14*, *20*, *37*, *38*), a region in the *p*FNR flavin binding domain containing two critical lysine residues, Lys85 and Lys88 (spinach numbering), was identified as the major site for interaction with Fd (*22*). The crystal structure of the complex between maize leaf *p*FNR and Fd confirmed the involvement of these lysine residues and identified additional salt bridges between Fd and *p*FNR, mediated by the *p*FNR residues Lys33, Lys81, Lys91, Lys 304, and Glu154 (*16*). The N-terminal of *p*FNR was too flexible to be resolved in detail in this crystal structure, but residues in this region important to Fd binding have been identified by NMR analysis and by truncation studies of the flexible N-terminal region of maize *p*FNRII. More specifically, interaction with Fd at the motifs EAxxPA and KxSKK (*19*), equivalent to regions located at the [N+22] and the N-terminal cleavage site of wheat *p*FNRII, respectively, have been proposed. These motifs are consistently found in other forms of *p*FNR (Figure 1).

The longer *p*FNRII N-terminal forms, *p*FNRII[N+22]$_{AQVS}$, *p*FNRII[N+8]$_{AAPA}$, and *p*FNRII[N+2]$_{VKIS}$, bound more tightly to the Fd column than did *p*FNRII$_{ISKK}$ and *p*FNRII-[N−2]$_{KKQD}$, which have been previously identified as representing two alternative N-terminal variants found *in vivo* (*9*). This suggests that the protein−protein interactions of Fd and *p*FNRII determined by Fd-affinity chromatography are markedly affected by N-terminal truncation of FNR. These results further support the suggestion that the N-terminal region contains residues which aid the binding of Fd to *p*FNR. In previous work, two N-terminally truncated forms of maize leaf *p*FNRII shortened to remove the EAxxPA or the KxSKK motif in the N-terminal region also exhibited a decreased affinity for a Fd affinity column (*19*). The removal of the wheat KISKK motif to generate *p*FNRII[N−5]$_{DEGV}$ resulted in a form of *p*FNRII that failed to bind to the Fd column altogether. Based on activity measurements made using a cytochrome *c* reduction enzyme assay, *p*FNRII[N−5]$_{DEGV}$ had a markedly reduced k_{cat} when compared to the other forms of *p*FNRII. The apparent K_m values for *p*FNRII$_{ISKK}$ and *p*FNRII[N−2]$_{KKQD}$ binding to FdI have previously been reported to be 28.6 and 8.35 μM, respectively (*9*). The comparable K_m values for the alternative truncated forms of *p*FNRII reported here were in the range 9.99−14.71 μM, apart from the longer *p*FNRII N-terminal form, *p*FNRII[N+22]$_{AQVS}$, which had a lower K_m of 3.12 μM. The data thus suggest some variations in the affinity of the various truncated *p*FNRII proteins for FdI based on K_m values from steady-state kinetic analysis. However, these are approximations to the K_d values, and further studies are required to ensure that the K_m values reflect accurately the K_d values.

In addition to complex formation between *p*FNRII and Fd, the role of the N-terminal region of *p*FNRII in electron transfer could have important regulatory implications. The impact of N-terminal truncations on electron flow was assessed by using

stopped-flow kinetic studies. Considerable alterations in the limiting rate of electron transfer (k_{obs}) between the various *p*FNRII proteins and Fd were observed, with the k_{obs} varying between 76 and 265 s^{-1} according to the extent of truncation and the secondary mutations introduced. Thus, N-terminal truncation of *p*FNRII does appear to influence intermolecular electron transfer between Fd_{red} and $pFNRII_{ox}$. This may reflect alterations in the orientation of the complexes (transient or otherwise) formed between the *p*FNRII and Fd proteins, preventing optimal intercofactor electron transfer. Small alterations to distance constraints may underlie these changes, since the differences in the potentials of the FAD cofactor, relative to that of the Fd iron−sulfur center, are not substantially modified.

The stopped-flow experiments suggest that all *p*FNRII enzymes measured have a high catalytic competence in transferring electrons to FdI at concentrations of 25 μM and above (Table 2). These experiments suggest that truncation and site-directed mutagenesis did not influence apparent affinity for FdI, since k_{obs} for electron transfer was constant in the FdI concentration range tested, although considerable variations in the k_{obs} value were determined (from 75.7 to 264.6 s^{-1}) dependent on the particular *p*FNRII isoform studied. These differences in the rates of interprotein electron transfer should, at least in part, explain the differences in steady-state cytochrome *c* reductase activity seen in Tables 1 and 4. The Fd-column chromatography method is a useful probe of affinity of the various *p*FNRII proteins for Fd, with differences in affinity likely based largely on altered electrostatics, as evident from altered salt elution profiles. In this way, changes in sensitivity of the complex between the oxidized forms of the *p*FNRII/Fd proteins were revealed by the variable salt concentrations of protein elution. In the stopped-flow transient kinetic studies, a relatively high initial concentration of Fd was used to maintain pseudo-first-order conditions, and excess salt was avoided to facilitate good complex formation between *p*FNRII and Fd proteins, so the impact of variable Fd binding is not readily measurable. These data indicate that at physiological ionic strength (approximately 100 mM NaCl) there is a substantial influence on the efficiency of complex formation between the various forms of *p*FNRII and Fd. This correlates with steady-state enzyme kinetic measurements and would lead to considerable differences in the efficiency of electron transport *in vivo*. In the chloroplast, the presence of a wide range of other proteins competing for the reduced Fd might also mean that any decreased affinity for *p*FNRII could result in marked changes to electron channeling into distinct pathways. The location of *p*FNR, bound to PSI at the end of the photosynthetic electron transfer chain, is a key position for regulating the flow of electrons. As such, *p*FNR catalyzes reactions where most of the reductant supply is converted into NADPH for carbon fixation via linear electron flow. This has a key effect on the downstream availability of reduced Fd for cyclic electron flow and also alternative electron flow, including processes such as nitrite reduction and ammonium assimilation (*4*−*6*, *39*). The demands of alternative electron flow for reduced Fd will also change with varying conditions, for example, nitrate supply and amino acid production.

The results presented in this paper provide further support for the view that the flexible N-terminal region of wheat *p*FNRII is important in the binding of Fd and may also influence the intercofactor electron transfer rate. However, as the EAxxPA motif is prior to the identified cleavage site in wheat, it is difficult to envisage this motif playing a significant role *in vivo*. In contrast, the truncation in the wheat KISKK motif leads to a *p*FNRII mutant ($pFNRII[N-5]_{DEGV}$) that totally loses binding capacity to a Fd chromatography column. Since this segment covers residues within the region of the two alternative N-terminal variants, $pFNRII_{ISKK}$ and $pFNRII[N-2]_{KKQD}$, identified by Gummadova and co-workers (*9*) as being present *in vivo*, then this could be of physiological importance for *in vivo* Fd interactions.

In previous work examining the spinach and maize *p*FNR proteins, lysine residues were identified as being particularly important in influencing Fd binding to FNR (*19*). Within the KISKK motif of wheat *p*FNRII there are three lysine residues which were targeted for site-directed mutagenesis. The lysine residues were changed to glutamines giving $pFNRII[N+22]_{AQVS}$ $K^{+1}Q$, $pFNRII[N+22]_{AQVS}$ $K^{-2}Q$, and $pFNRII[N+22]_{AQVS}$ $K^{-2}K^{-3}QQ$ variants. In all cases the mutagenesis led to a decrease in affinity for the immobilized Fd column and a diminished catalytic efficiency when compared to the wild-type form $pFNRII[N+22]_{AQVS}$, as investigated by steady-state enzyme assays. The catalytic mechanism whereby reduced Fd and $NADP^+$ both bind to the active site of FNR was first proposed by Batie and Kamin (*18*). As the complex between FNR and Fd is largely electrostatic, the basic charges in the lysine side chains of the N-terminal region of *p*FNR are needed for the formation of the FNR:Fd intermediate complex (*19*, *38*). This suggests that the lysine residues identified in the N-terminal region of the wheat *p*FNRII play an important role in the interaction with Fd.

Clearly, truncation has an impact on the *in vitro* binding of *p*FNRII and Fd. Such truncations could thus have an impact on the effective flow of electrons through specific metabolic pathways *in vivo* and also be affected by alterations in physiological conditions, such as the ionic environment. Although we do not yet know whether specific isoforms of *p*FNR are catalytically more likely to channel electrons into specific metabolic processes, terminal truncation could provide the leaf with the flexibility to produce multiple forms of *p*FNR which preferentially respond to changes in reductant demand and, depending on the photosynthetic status of the cell, are able to alter the balance between cyclic and noncyclic electron flow. In studies using *Arabidopsis* mutant lines, both *p*FNR forms are needed for optimal growth. The absence of either form leads to a decrease in chlorophyll content, the low accumulation of photosynthetic thylakoid proteins, and a decreased carbon fixation rate (*5*). The absence of *p*FNRI provided *Arabidopsis* plants with tolerance to oxidative stress (*5*). In addition, the absence of *p*FNRII resulted in *Arabidopsis* plants with altered electron channeling leading to increased biomass when grown under low nitrate conditions (*4*). In contrast to *Arabidopsis*, where only two forms of *p*FNR have been identified *in vivo*, N-terminal truncation of wheat *p*FNR forms provides a further level of regulation. As a shade plant exposed to less variation in growth light, *Arabidopsis* metabolism probably has a lower demand for cyclic flow. In wheat grown under conditions which impact on photosynthetic capacity, truncation of *p*FNR *in vivo* could provide additional flexibility to regulate catalytic capacity.

SUPPORTING INFORMATION AVAILABLE

Figures S1A and S1B showing SDS−PAGE and native PAGE gel patterns of the purified *p*FNRII forms, stained with Coomassie Brilliant Blue or for FNR activity, respectively. This material is available free of charge via the Internet at http://pubs.acs.org.

REFERENCES

1. Carrillo, N., and Ceccarelli, E. A. (2003) Open questions in ferredoxin-NADP$^+$ reductase catalytic mechanism. *Eur. J. Biochem. 270*, 1900–1915.
2. Ceccarelli, E. A., Arakaki, A. K., Cortez, N., and Carrillo, N. (2004) Functional plasticity and catalytic efficiency in plant and bacterial ferredoxin-NADP(H) reductases. *Biochim. Biophys. Acta 1698*, 155–165.
3. Arakaki, A. K., Ceccarelli, E. A., and Carrillo, N. (1997) Plant-type ferredoxin-NADP$^+$ reductases: a basal structural framework and a multiplicity of functions. *FASEB J. 11*, 133–140.
4. Hanke, G. T., Endo, T., Satoh, F., and Hase, T. (2008) Altered photosynthetic electron channelling into cyclic electron flow and nitrite assimilation in a mutant of ferredoxin: NADP(H) reductase. *Plant Cell Environ. 31*, 1017–1028.
5. Lintala, M., Allahverdiyeva, Y., Kangasjarvi, S., Keranen, M., Rintamaki, E., Aro, E.-M., and Mulo, P. (2009) Comparative analysis of leaf-type ferredoxin-NADP$^+$ oxidoreductase isoforms in *Arabidopsis thaliana*. *Plant J. 57*, 1103–1115.
6. Moolna, A., and Bowsher, C. G. (2010) The physiological importance of photosynthetic ferredoxin NADP$^+$ oxidoreductase (FNR) isoforms in wheat. *J. Exp. Bot. 61*, 2669–2681.
7. Okutani, S., Hanke, G. T., Satomi, Y., Takao, T., Kurisu, G., Suzuki, A., and Hase, T. (2005) Three maize leaf ferredoxin: NADPH oxidoreductases vary in subchloroplast location, expression, and interaction with ferredoxin. *Plant Physiol. 139*, 1451–1459.
8. Rodriguez, R. E., Lodeyro, A., Poli, H. O., Zurbriggen, M., Peisker, M., Palatnik, J. F., Tognetti, V. B., Tschiersch, H., Hajirezaei, M.-R., Valle, E. M., and Carrillo, N. (2007) Transgenic tobacco plants overexpressing chloroplastic ferredoxin-NADP(H) reductase display normal rates of photosynthesis and increased tolerance to oxidative stress. *Plant Physiol. 143*, 639–649.
9. Gummadova, J. O., Fletcher, G. J., Moolna, A., Hanke, G. T., Hase, T., and Bowsher, C. G. (2007) Expression of multiple forms of ferredoxin NADP(+) oxidoreductase in wheat leaves. *J. Exp. Bot. 58*, 3971–3985.
10. Matsumura, T., Kimata-Ariga, Y., Sakakibara, H., Sugiyama, T., Murata, H., Takao, T., Shimonishi, Y., and Hase, T. (1999) Complementary DNA cloning and characterization of ferredoxin localized in bundle-sheath cells of maize leaves. *Plant Physiol. 119*, 481–488.
11. Kimata-Ariga, Y., Matsumura, T., Kada, S., Fujimoto, H., Fujita, Y., Endo, T., Mano, J., Sato, F., and Hase, T. (2000) Differential electron flow around photosystem I by two C-4-photosynthetic-cell-specific ferredoxins. *EMBO J. 19*, 5041–5050.
12. Martínez-Júlvez, M., Nogués, I., Faro, M., Hurley, J. K., Brodie, T. B., Mayoral, T., Sanz-Aparicio, J., Hermoso, J. A., Stankovich, M. T., Medina, M., Tollin, G., and Gómez-Moreno, C. (2001) Role of a cluster of hydrophobic residues near the FAD cofactor in *Anabaena* PCC 7119 ferredoxin-NADP$^+$ reductase for optimal complex formation and electron transfer to ferredoxin. *J. Biol. Chem. 276*, 27498–27510.
13. Martínez-Júlvez, M., Medina, M., Hurley, J. K., Hafezi, R., Brodie, T. B., Tollin, G., and Gómez-Moreno, C. (1998) Lys75 of *Anabaena* ferredoxin-NADP$^+$ reductase is a critical residue for binding ferredoxin and flavodoxin during electron transfer. *Biochemistry 37*, 13604–13613.
14. Aliverti, A, Corrado, M. E., and Zanetti, G. (1994) Involvement of lysine-88 of spinach ferredoxin-NADP$^+$ reductase in the interaction with ferredoxin. *FEBS Lett. 343*, 247–250.
15. Morales, R., Chanon, M.-H., Kachalova, G., Serre, L., Medina, M., Gomez-Moreno, C., and Frey, M. (2000) A redox-dependent interaction between two electron transfer partners involved in photosynthesis. *EMBO Rep. 1*, 271–276.
16. Kurisu, G., Kusunoki, M., Katoh, E., Yamazaki, T., Teshima, K., Onda, Y., Kimata-Ariga, Y., and Hase, T. (2001) Structure of the electron transfer complex between ferredoxin and ferredoxin-NADP$^+$ reductase. *Nat. Struct. Biol. 8*, 117–121.
17. Smith, J. M., Smith, W. H., and Knaff, D. B. (1981) Electrochemical titrations of a ferredoxin-ferredoxin-NADP$^+$ reductase complex. *Biochim. Biophys. Acta 635*, 405–411.
18. Batie, C. J., and Kamin, H. (1984) Ferredoxin-NADP$^+$ oxidoreductase. Equilibria in binary and ternary complexes with NADP$^+$ and ferredoxin. *J. Biol. Chem. 259*, 8823–8839.
19. Maeda, M., Lee, Y. H., Ikegami, T., Tamura, K., Hoshino, M., Yamazaki, T., Nakayama, M., Hase, T., and Goto, Y. (2005) Identification of the N- and C-terminal substrate binding segments of ferredoxin-NADP$^+$ plus reductase by NMR. *Biochemistry 44*, 10644–10653.
20. Aliverti, A., Jansen, T., Zanetti, G., Ronchi, S., Herrmann, R. G., and Curti, B. (1990) Expression in *Escherichia coli* of ferredoxin:NADP$^+$ reductase from spinach. Bacterial synthesis of the holoflavoprotein and of an active enzyme form lacking the first 28 amino acid residues of the sequence. *Eur. J. Biochem. 191*, 551–555.
21. Gadda, G., Aliverti, A., Ronchi, S., and Zanetti, G. (1990) Structure-function relationship in spinach ferredoxin-NADP$^+$ reductase as studied by limited proteolysis. *J. Biochem. 265*, 11955–11959.
22. Zanetti, G., Morelli, D., Ronchi, S., Negri, A., Aliverti, A., and Curti, B. (1988) Structural studies on the interaction between ferredoxin and ferredoxin-NADP$^+$ reductase. *Biochemistry 27*, 3753–3759.
23. Onda, Y., Matsumura, T., Kimata-Ariga, Y., Sakakibara, H., Sugiyama, T., and Hase, T. (2000) Differential interaction of maize root ferredoxin:NADP(+) oxidoreductase with photosynthetic and non-photosynthetic ferredoxin isoproteins. *Plant Physiol. 123*, 1037–1046.
24. Dutton, P. L. (1978) Redox potentiometry: determination of midpoint potentials of oxidation-reduction components of biological electron-transfer systems. *Methods Enzymol. 54*, 411–435.
25. Munro, A. W., Noble, M. A., Robledo, L., Daff, S. N., and Chapman, S. K. (2001) Determination of the redox properties of human NADPH-cytochrome P450 reductase. *Biochemistry 40*, 1956–1963.
26. Lawson, R. J., von Wachenfeldt, C., Haq, I., Perkins, J., and Munro, A. W. (2004) Expression and characterization of the two flavodoxin proteins of *Bacillus subtilis*, *YkuN* and *YkuP*: biophysical properties and interactions with cytochrome P450. *Biochemistry 43*, 12390–12409.
27. Daff, S. N., Chapman, S. K., Turner, K. L., Holt, R. A., Govindaraj, S., Poulos, T. L., and Munro, A. W. (1997) Redox control of the catalytic cycle of flavocytochrome P-450 BM3. *Biochemistry 36*, 13816–13823.
28. McLean, K. J., Warman, A. J., Seward, H. E., Marshall, K. R., Girvan, H. M., Cheesman, M. R., Waterman, M. R., and Munro, A. W. (2006) Biophysical characterization of the sterol demethylase P450 from *Mycobacterium tuberculosis*, its cognate ferredoxin, and their interactions. *Biochemistry 45*, 8427–8443.
29. McIver, L., Leadbeater, C., Campopiano, D. J., Baxter, R. L., Daff, S. N., Chapman, S. K., and Munro, A. W. (1998) Characterisation of flavodoxin NADP(+) oxidoreductase and flavodoxin; key components of electron transfer in *Escherichia coli*. *Eur. J. Biochem. 257*, 577–585.
30. Cidaria, D., Biondi, P. A., Zanetti, G., and Ronchi, S. (1985) The NADP$^+$-binding site of ferredoxin-NADP$^+$ reductase. Sequence of the peptide containing the essential lysine residue. *Eur. J. Biochem. 146*, 295–299.
31. Jelesarov, I., De Pascalis, A. R., Koppenol, W. H., Hirasawa, M., Knaff, D. B., and Bosshard, H. R. (1993) Ferredoxin binding site on ferredoxin:NADP$^+$ reductase. Differential chemical modification of free and ferredoxin-bound enzyme. *Eur. J. Biochem. 216*, 57–66.
32. Orellano, E. G., Calcaterra, N. B., Carrillo, N., and Ceccarelli, E. A. (1993) Probing the role of the carboxyl-terminal region of ferredoxin-NADP$^+$ reductase by site-directed mutagenesis and deletion analysis. *J. Biol. Chem. 268*, 19267–19273.
33. Medina, M., Mendez, E., and Gómez-Moreno, C. (1992a) Identification of arginyl residues involved in the binding of ferredoxin-NADP$^+$ reductase from *Anabaena* sp. PCC 7119 to its substrates. *Arch. Biochem. Biophys. 299*, 281–286.
34. Medina, M., Mendez, E., and Gómez-Moreno, C. (1992b) Lysine residues on ferredoxin-NADP$^+$ reductase from *Anabaena* sp. PCC 7119 involved in substrate binding. *FEBS Lett. 298*, 25–28.
35. Aliverti, A., Liibberstedtg, T., Zanetti, G., Herrmanns, R. G., and Curti, B. (1991) Probing the role of lysine 116 and lysine 244 in the spinach ferredoxin-NADP$^+$ reductase by site-directed mutagenesis. *J. Biol. Chem. 266*, 17760–17763.
36. Bruns, C. M., and Karplus, P. A. (1995) Refined crystal structure of spinach ferredoxin reductase at 1.7 Å resolution: oxidized, reduced and 2′-phospho-5′-AMP bound states. *J. Mol. Biol. 247*, 125–145.
37. Medina, M., and Gómez-Moreno, C. (2004) Interaction of ferredoxin-NADP(+) reductase with its substrates: optimal interaction for efficient electron transfer. *Photosynth. Res. 79*, 113–131.
38. Hurley, J. K., Hazzard, J. T., Martinez-Julvez, M., Medina, M., Gomez-Moreno, C., and Tollin, G. (1999) Electrostatic forces involved in orienting *Anabaena* ferredoxin during binding to *Anabaena* ferredoxin-NADP$^+$ reductase: site directed mutagenesis, transient kinetic measurements and electrostatic surface. *Protein Sci. 8*, 1614–1622.
39. Lintala, M., Allahverdiyeva, Y., Kidron, H., Piippo, M., Battchikova, N., Suorsa, M., Rintamaki, E., Salminen, T. A., Aro, E. M., and

Mulo, P. (2007) Structural and functional characterization of ferredoxin-$NADP^+$-oxidoreductase using knock-out mutants of Arabidopsis. *Plant J. 49*, 1041–1052.
40. Jansen, T., Reilander, H., Steppuhn, J., and Herrmann, R. G. (1988) Analysis of cDNA clones encoding the entire precursor-polypeptide for ferredoxin:$NADP^+$ oxidoreductase from spinach. *Curr. Genet. 13*, 517–522.
41. Newman, B. J., and Gray, J. C. (1988) Characterisation of a full length cDNA clone for ferredoxin $NADP^+$ oxidoreductase. *Plant Mol. Biol. 10*, 511–520.